

Efficient and Tunable Photochemical Charge Transfer via Long-Lived Bloch Surface Wave Polaritons

Kamyar Rashidi,^{1,2,*} Evripidis Michail,^{1,2} Bernardo Salcido-Santacruz,^{1,3}
Yamuna Paudel,^{1,2} Vinod M. Menon,^{2,4} and Matthew Y. Sfeir^{1,2,†}

¹*Photonics Initiative, Advanced Science Research Center,
City University of New York, New York, New York 10031, USA*

²*Department of Physics, Graduate Center, City University of New York, New York, New York 10016, USA*

³*Department of Chemistry, Graduate Center, City University of New York, New York, New York 10016, USA*

⁴*Department of Physics, City College of New York, New York, New York 10031, USA*

(Dated: September 4, 2024)

Achieving precise control of photoinduced molecular charge transfer reactions underpins key emerging technologies. As such, the use of hybrid light-matter molecular exciton-polariton states has been proposed as a scheme to directly modify the efficiency and rate of such reactions. However, the efficacy of polariton-driven photochemistry remains an open question. Here, we demonstrate conditions under which photoinduced polaritonic charge transfer can be achieved and directly visualized using momentum resolved ultrafast spectroscopy. Key conditions for charge transfer are satisfied using Bloch surface wave polaritons, which exhibit favorable dispersion characteristics that permit the selective pumping of hybrid states with long lifetimes (100-400 fs) that permit vibrationally assisted molecular charge transfer. Using this approach, we tune the energetic driving force for charge separation, reducing it by as much as 0.5 eV compared to the bare exciton. These results establish that tunable and efficient polariton-driven molecular charge transfer is indeed possible using carefully considered photonic systems.

Organic exciton polaritons emerge due to strong coupling between the excitonic states of organic materials and the electromagnetic modes of optical cavities, creating hybrid quasiparticles with both matter and photon characteristics[1, 2]. A key advantage of organic materials in strong light-matter coupling applications is that they enable the investigation of novel quantum states at room temperature[3], including such phenomena as polariton condensation[4], superfluidity[5], and soliton propagation[6]. In addition, due to their strong absorption, large delocalization, and tunable energetics, organic exciton-polaritons have also been widely proposed as attractive candidates for applications involving photoinduced charge transfer (CT), such as optoelectronics, spin conversion processes, and isomerization reactions[7–16].

The potential advantages of polariton photochemistry have been widely championed [17–20]. In the field of molecular photochemistry, a great deal of effort is devoted to engineering the reactivity of the excited state by tuning its potential energy surface and the character of the its wavefunction. For example, the conversion from a bound excitonic to an unbound charge separated state requires a energetic driving force[21, 22] (Fig. 1a) that is generally provided in the form of a chemical potential difference between an excited state of an absorbing donor molecule and an unoccupied molecular orbital of an acceptor compound. In this con-

text, polariton-driven photochemistry would uniquely enable a means of dynamically tuning excited state potentials via dispersion of the hybrid state without modification of the molecular structure (Fig. 1b). This potentially allows for the determination of electronic and kinetic factors that dictate charge transfer reactions[23], photoisomerizations[24], and spin conversion processes among others[25, 26]. If realized, the phenomena of tunable polariton photochemistry could have an impact analogous to the scientific revolution enabled by the size and shape dependent properties of quantum-confined nanomaterials.

However, fundamental challenges have so far precluded the realization of dynamically tunable exciton polariton-based photochemical systems. The lack of a consensus as to the efficacy of organic exciton-polariton photochemistry is rooted in several factors that affect the understanding of their excited state dynamics and has hindered the reproducibility of many studies. One issue is that in molecular systems, charge-transfer processes are generally understood within the context of Marcus Theory, which described how changes in the spatial charge distribution are stabilized by corresponding changes in the nuclear coordinates (Fig. 1a)[27, 28]. As such, the rate of CT is fundamentally limited by the atomic motion rather than the electron tunneling time[29]. In other words, for intermolecular CT to proceed efficiently, the lifetime of the excited donor state ($1/\gamma_r$) must exceed the timescale for nuclear reorganization ($1/\gamma_Q$), whose lower limit is on the order of 100 fs [30]. Notably, this condition is not always met under strong coupling conditions. For example, typical all-metal microcavities exhibit fast momentum scattering (γ_k) and photon lifetimes of < 25 fs (Fig. 1c). These short lifetimes likely preclude effi-

* Photonics Initiative, Advanced Science Research Center, City University of New York, New York, New York 10031, USA; Department of Physics, Graduate Center, City University of New York, New York, New York 10016, USA

† msfeir@gc.cuny.edu

cient CT, even under conditions where selective exciton-polariton excitation is achieved [31, 32].

Additionally, to understand the dynamics of polariton photochemistry, it is necessary to distinguish between CT resulting from hybrid states compared to matter states[33, 34]. This is particularly challenging in organic systems where a large amount of inhomogeneous broadening together with strong electron-vibrational coupling imparts significant oscillator strength to reservoir states[35, 36]. These states are formally linear combinations of exciton basis states, and it has been experimentally shown that their energies, potential energy surfaces, and dynamics are largely identical to bare, uncoupled excitons[35–37]. However, distinguishing between polariton and reservoir state dynamics can be very challenging since energy storage in reservoir states leads to spurious transient signals at polariton resonances. These signals result from small changes in the photonic properties of the system, but are frequently misinterpreted and incorrectly used to assign polariton lifetimes[38–40]. This problem can be addressed by selecting a photonic system with a dispersion suitable for selective excitation of polaritons. For example, we have shown in recent work that the steep dispersion associated with surface and waveguide modes permit selective excitation of hybrid states via their energy- and momentum-resonance conditions and permits a direct measurement of its decay dynamics[32]. Still, it remains a grand challenge to demonstrate that the rate and efficiency of photochemical processes based on CT are inherently impacted by the presence of hybrid polariton states.

We posit that to fully identify and understand the dynamics of polariton-driven photochemical processes, it is therefore necessary to achieve both selective excitation of exciton-polaritons and exciton-polariton lifetimes that exceed the characteristic timescale for nuclear relaxation. To test this, we leverage the favorable properties of organic materials strongly coupled to Bloch surface waves (BSW). The advantages of this system has been recently demonstrated to include their exceptionally high group velocity, prolonged lifetime, and minimal dissipation that have led to long propagation distances at room temperature[41–46]. For the purposes of CT, the simple geometry and long lifetimes are promising for mechanistic studies of polariton mediated charge transfer. Furthermore, we are able to take advantage of the dispersion of BSW-polaritons to selectively excite the lower polariton (LP) state under energy- and momentum-matching conditions. Here we show that polariton-enhanced CT can indeed be achieved under these specific conditions using a strongly coupled organic donor molecular and a molecular acceptor through the identification of ion states that are resonantly generated on ultrafast timescales. Importantly, CT is not achieved in analogous metallic cavities with similar dispersion properties due to their short lifetimes relative to nuclear relaxation. We show that the dynamics of BSW-polaritons can be observed through both LP and Internal Optical Modes (IOMs) and that

significant quenching of the polariton emission signal is observed in the CT regime. Ultimately, we achieve efficient and tunable CT using the LP-BSW Mode and show that the overpotential for CT can be reduced by as much as 0.5 eV.

I. Photonic structure design considerations

Our photonic structure with long-lived exciton-polariton states consists of an 80 nm layer of organic dye encapsulated in a polymethyl methacrylate (PMMA) matrix that is deposited on the surface of a one dimensional photonic crystal comprised of six pairs of alternating Si_3N_4 (110 nm) / SiO_2 (146 nm) layers (Fig. 1c (right)). The organic layer consists of either Pyrromethene 605 donor molecules (PM605), Tetracyanoquinodimethane acceptor molecules (TCNQ), or a mixture of both the donor and acceptor in a 1:1 ratio (PM605-TCNQ 1:1). A BSW mode located within the photonic bandgap gives rise to a confined electric field in the immediate vicinity of the surface. Spatial overlap of the confined electromagnetic field and the strongly absorbing organic dye leads to strong light-matter coupling and the formation of exciton-polaritons with a large Rabi splitting ($\hbar\Omega \propto (N/V_m)^{1/2}$), where V_m is the effective mode volume and N is the number of coupled molecules. In the strong coupling regime, the polariton lifetime will be limited by the uncoupled photonic lifetime through $\tau_{xp}^{-1} = A\tau_p^{-1} + B\tau_x^{-1}$, where τ_p and τ_x are the lifetimes of the uncoupled photonic and excitonic states, and A and B are their respective fractions in the wavefunction. Here, the quality factor (Q -factor) of the uncoupled photonic BSW mode, in which the organic layer consists of only the PMMA matrix, is calculated using transfer matrix methods to be approximately 366, corresponding to $\tau_p > 125$ fs (Fig. 1d). This lifetime is significantly longer than corresponding modes in other common photonic systems, such as surface plasmon polaritons where $\tau_p < 10$ fs as well as metal microcavity and waveguide modes in which $\tau_p < 25$ fs[32]. These differences in the relaxation times are extremely significant in the context of molecular CT. For photonic systems in which the lifetime of the photonic state is shorter than what is required for vibrationally-mediated charge transfer, charge separation is suppressed due to rapid ground state recovery (Fig. 1c (left)). In contrast, BSW and other high- Q photonic systems exhibit higher τ_p , such that incoherent CT processes become accessible (Fig. 1c (right)). As such, similar to the case of a bare exciton, a long LP lifetime is necessary to facilitate CT from a hybrid light-matter state.

II. Charge transfer in the bare D-A film

Steady-state and transient optical spectroscopy combined with spectroelectrochemical measurements confirm that rapid and efficient formation of a charge separated

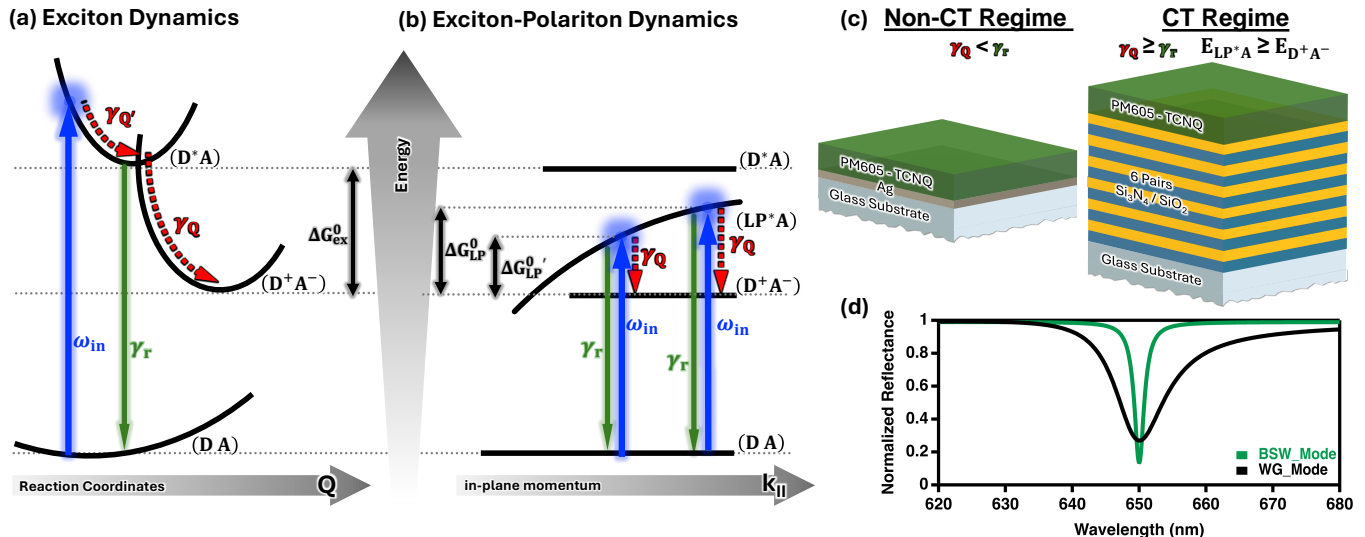


FIG. 1. **Charge Transfer (CT) Processes in Donor-Acceptor Systems: Bare vs. Metal and DBR Cavities.** Schematic representation of photon absorption from the ground state (GS, DA) with energy $\hbar\omega_{in}$ to the excited state of the (a) bare donor-acceptor system (D^*A) and (b) cavity donor-acceptor system (LP^*A). Two competing pathways of relaxation to the ground state and transfer to the charge-transfer state (D^+A^-) are shown with their respective rate constants (γ_r and γ_e) where the arrows represent population transfer. For bare excitons, the driving force (ΔG_{ex}^0) remains constant and relatively high. However, with polaritons, this value can be adjusted to various lower levels, represented by ΔG_{LP}^0 and $\Delta G_{LP'}^0$. (c) Left: A metal cavity structure composed of a 150 nm PM605-TCNQ film spin-coated onto a 30 nm silver layer. Due to the lower lifetime (lower Q-factor) of the polariton state, electron relaxation to the ground state occurs before charge transfer can happen. (c) Right: A photonic structure composed of an 80 nm PM605-TCNQ film spin-coated onto six pairs of Si_3N_4 (110 nm)/ SiO_2 (146 nm) dielectric Bragg reflectors. The longer lifetime (higher Q-factor) of the polariton state in this structure allows for charge transfer to occur. (d) Reflection spectra of the uncoupled waveguide (WG) mode in metallic cavity and BSW in distributed Bragg reflector (DBR) cavities were obtained using the transfer matrix method. The Q-factors for the WG mode and BSW were measured as 73 and 366, respectively.

state occurs in the PM605-TCNQ blend outside of the cavity. The absorption spectrum of the blend largely resembles a linear combination of the individual components (Fig. 2a), with the neutral PM605 and TCNQ components identified by their distinct absorption profiles at 550 nm and 400 nm, respectively. Notably, the emission spectra of the PM605-TCNQ blend (inset of Fig. 2a) show strong quenching relative to a neat PM605 film. The energies of the frontier molecular orbitals determined from cyclic voltammetry suggest that a large (~ 700 meV) energetic driving force facilitates excited state electron transfer from the PM605 exciton to the TCNQ (Fig. S1). The corresponding ion spectra (Fig. 2b) indicate that $TCNQ^-$ exhibits strong characteristic absorption peaks at 744 nm and 843 nm. While PM605⁺ does not exhibit a characteristic transition in our spectral window, the neutral absorption peak of PM605 at 542 nm is largely suppressed upon ionization. Transient optical studies performed on films of the individual components and their blend confirm that ultrafast electron transfer dynamics occur in the blend upon photoexcitation (Fig. S2), Fig. 2c). These measurements (Fig. 2c) reveal a concurrent decay of ground state bleach of PM605 around 590 nm and the rise of excited state absorption (ESA) around 780 nm and 850 nm corresponding to anion for-

mation ($TCNQ^-$). From an analysis of the kinetics, we determine that CT occurs within 180 fs resulting in an anion lifetime of 5.41 ps.

III. Momentum-resolved exciton-polariton dynamics

We identify that strong light-matter coupling is achieved between the PM605 exciton and the BSW mode when both the neat PM605 film and the PM605-TCNQ blend are deposited on our DBR structure. The angle-resolved reflectivity of PM605/DBR and PM605-TCNQ/DBR structures (Fig. 3a,b) illustrates the avoided crossing between the BSW mode (dashed black lines) and the exciton energy level (dashed red line near 542 nm) of PM605 above the critical angle ($\sim 40^\circ$). The resulting LP state (solid black line) can be seen as a dip in the reflectivity in both simulations and experiments. We note that the upper polariton is not readily identifiable within our measurement range. In addition to the BSW surface mode, the DBR exhibits several IOMs above and below the light line, for which the electric field is extended into either air or the dielectric stack (Fig. 3c). As we will show later, these modes are weakly coupled to the organic layer and exhibit a modified dispersion due to changes to the effec-

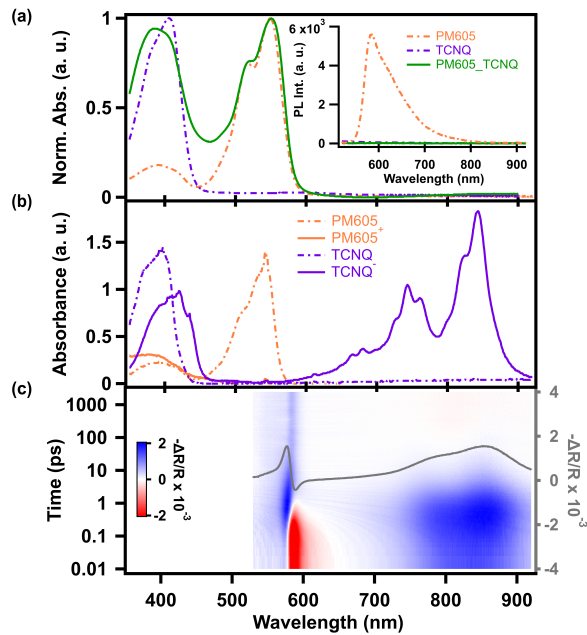


FIG. 2. **Highlighting CT Signatures in PM605-TCNQ Blend Film.** (a) Absorption of PM605, TCNQ, and their 1:1 mixture PM605-TCNQ. The inset displays the emission spectra, where emission is quenched for the PM605-TCNQ blend film. (b) Steady-state absorption spectra of PM605, PM605⁺, TCNQ, and TCNQ⁻ in acetonitrile measured using spectroelectrochemical techniques. TCNQ⁻ exhibits two additional anion absorption peaks at 744 nm and 843 nm. PM605 has a peak at 542 nm, which is quenched for its cation (PM605⁺). (c) Transient reflection spectra of the PM605-TCNQ 1:1 mixture. The secondary vertical axis represents the average transient reflection from 0.1 to 4 ps, revealing excited state absorption around the anion absorption, as well as quenching of the ground state bleach near the PM605 absorption.

tive refractive index of the organic layer in the excited state. The separation between the BSW and the LP indicates the strong coupling regime, satisfying the condition $\hbar\Omega_R \geq (\Gamma_M + \Gamma_C)/2$, where $\hbar\Omega_R$ denotes the Rabi splitting energy (585 meV), while Γ_M and Γ_C represent the full width at half maximum linewidths of the bare molecule exciton (255 meV) and the cavity mode (5.4 meV), respectively.

Selective excitation of the LP in transient optical measurements is accomplished using the Kretschmann-Raether attenuated total reflection approach that enables the excitation of BSWs from the far-field (Fig. 4a). Briefly, the optical pump and probe pulses propagate at high angles through a prism coupled to our photonic structure using index-matching oil. The two pulses are spatially overlapped on the active area of our structure with an angular offset of $\Delta\theta = \theta_{\text{pump}} - \theta_{\text{probe}}$ and a delay time of Δt . The broadband reflected probe signal detects transient changes in the refractive indices of the organic layer. As we have previously shown, selective excitation of LP states occurs under PMCs in which

the pump wavelength and angle are tuned to match the dispersion of the hybrid LP mode (Fig. S3)[32]. Direct measurements of the polariton lifetime are enabled by excitation at specific in-plane momenta that correspond to LPs with both significant excitonic character and a large energetic separation from reservoir states. On the other hand, excitation of reservoir states is accomplished by tuning the wavelength of the pump pulse to be resonant with the bare exciton energy. In contrast to polariton states, the excitation of reservoir states occurs for any value of the in-plane momentum of the pump pulse. We conducted our measurements within the low excitation regime (less than $4 \mu\text{J}/\text{cm}^2$), employing a high-sensitivity transient optical spectrometer recently developed by our group[47].

We established that the lifetime of the BSW exciton-polariton in the neat PM605 film exhibits long lifetimes that exceed the CT time constant that we measured in the uncoupled blend film (180 fs). As the lifetime of the exciton-polariton depends on the relative excitonic and photonic fractions, we tuned the energy and in-plane momentum of our pump pulse to resonantly excite various points on the LP dispersion curve. We performed this experiment under PMCs across three distinct wavelengths ($\lambda_{\text{pump}} = 650 \text{ nm}$, 680 nm , and 700 nm) with a consistent fluence ($1 \mu\text{J}/\text{cm}^2$) and a constant $\Delta\theta = 6.2^\circ$ (Fig. 4b). After photoexcitation, the transient spectra exhibit a dispersive shape centered at the LP transition energy, indicating a blue-shift of the hybrid mode in the excited state. Representative data with $\lambda_{\text{pump}} = 680 \text{ nm}$ are shown in Fig. 4, for which a strong dispersive feature associated with the LP appears near 735 nm. This response is characteristic of strongly-coupled systems and reflects a transient decrease in Rabi splitting due to the photoexcitation of a subset of coupled molecules. This effect is verified with power-dependent measurements, which show that the magnitude of the blue shift increases with increasing pump power (Fig. S4). The lifetime of the LP state is determined by measuring the timescale for the decay of the dispersive signal near the LP (Fig. 4d and f), which yields a decay constant of approximately 390 fs at the 650 nm pump wavelength. Importantly, this value is twice as long as the CT rate uncoupled PM605-TCNQ blend. As the in-plane momentum pump and probe momenta are decreased (shift of LP to longer wavelengths), the lifetime of LP decreases to $\sim 275 \text{ fs}$ at $\lambda_{\text{pump}} = 680 \text{ nm}$ and $\sim 150 \text{ fs}$ at $\lambda_{\text{pump}} = 700 \text{ nm}$, consistent with greater photonic character.

There are two other features that are readily apparent in the transient optical data, but are not relevant to the problem of photoinduced CT. At very early times ($< 200 \text{ fs}$) the sign of the dispersive signal is reversed, consistent with an optical Stark effect[48, 49]. This sign reversal induces an obvious oscillating component in the early time kinetics near the LP resonance (Fig. 4d) but doesn't affect our determination of the LP lifetime. In addition, a long-lived, non-dispersive signal with negative $-\Delta R/R$ is observed near the LP resonance that exhibits a lifetime

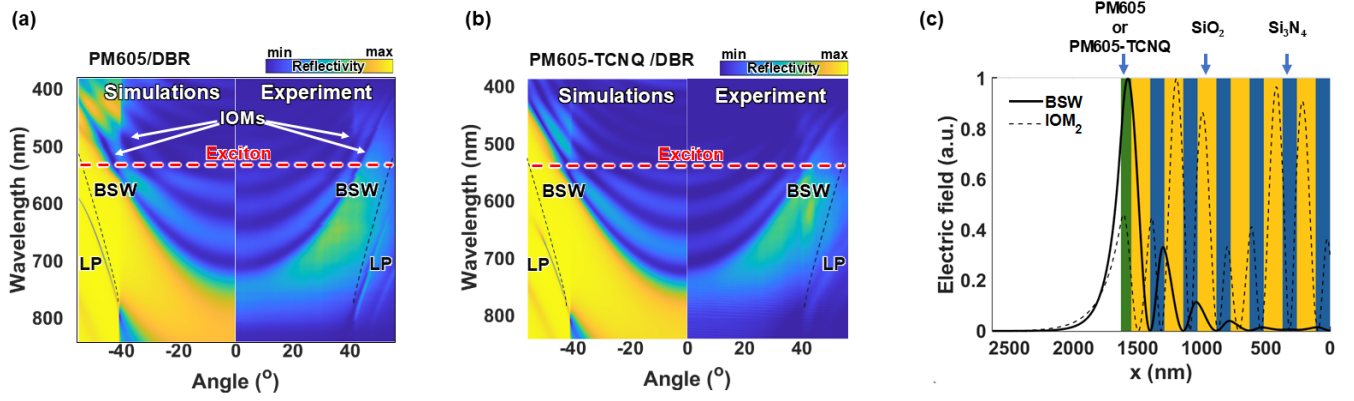


FIG. 3. **Strong coupling between the BSW mode and excitonic states.** Simulated (left) and measured (right) TE-polarized angle-resolved reflection spectra of (a) PM605/DBR and (b) PM605-TCNQ/DBR. The uncoupled exciton and BSW dispersions are represented by dashed red and black lines, respectively. (c) DBR configuration supporting in-plane propagating BSW and IOM₂ modes.

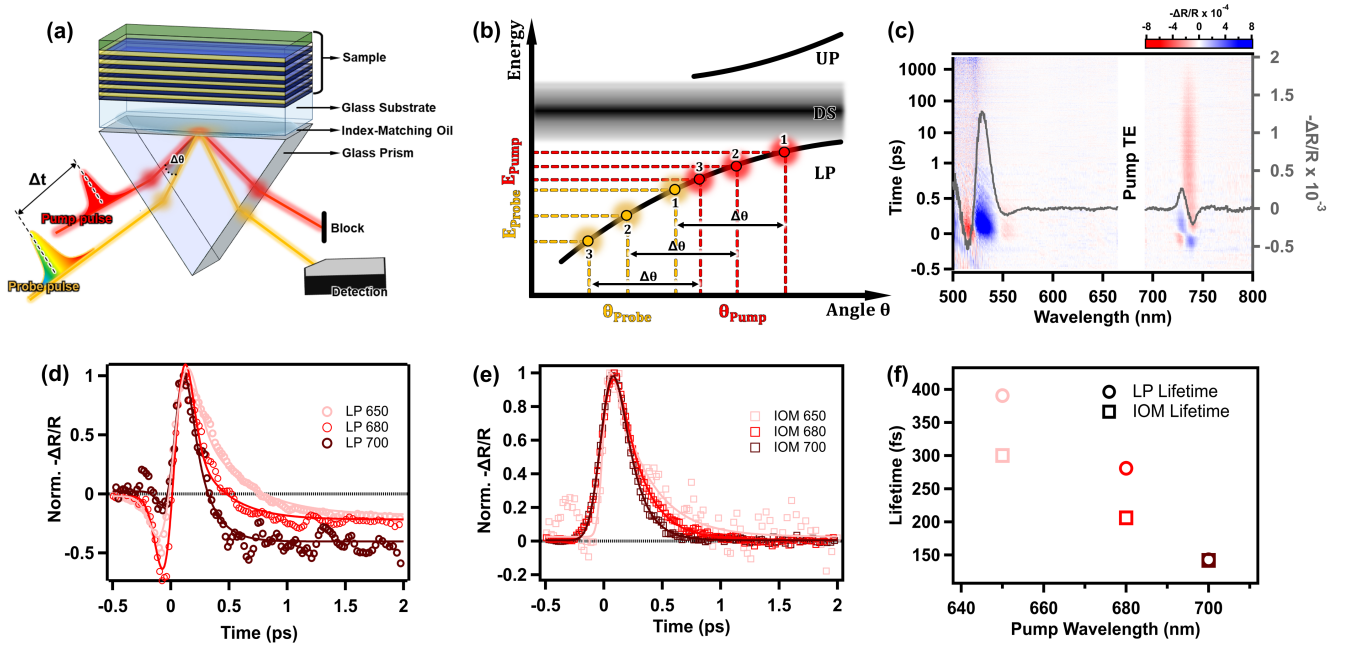


FIG. 4. **Lifetime of BSW polaritons across various points on the LP branch.** (a) Schematic representation of the pump-probe experimental configuration in the Kretschmann-Raether setup. The pump and probe beams are directed onto the sample with an angular difference $\Delta\theta = \theta_{\text{pump}} - \theta_{\text{probe}}$. The probe beam (white light) is delayed by a time Δt after the pump. The sample is positioned on top of the prism with index-matching oil, substrate side down. (b) Schematic diagram illustrating the excitation of LPs with three different pump wavelengths (650 nm, 680 nm, and 700 nm) under phase-matching condition (PMC), while maintaining a constant angle between the pump and probe beams ($\Delta\theta = 6.2^\circ$). (c) Transient reflection upon excitation with a 680 nm pump. The secondary vertical axis displays transient spectra within the first 200 fs. (d) Kinetic traces of LP and (e) IOMs for the three different pump wavelengths at the positions of gray dashed lines in (c). (f) Lifetimes of polariton and IOM corresponding to three different excitation wavelengths.

on the order of 200 ps, similar to the bare PM605 exciton (Fig. S2). Notably, the non-dispersive signals scale linearly with pump fluence and are spectrally distinct from the dispersive modes observed for reservoir pumping. Furthermore, they are not observed for an identical film

coupled to surface photonic modes of a metal film. As such, we assign this to weakly coupled stimulated emission originating from uncoupled molecules populated by long-range energy transfer. This emissive species likely originates from dye aggregates with red-shifted emission

that are observable only due to the low losses and large group velocities of the BSW mode. In this case, the polariton mode acts only as a spectral filter that facilitates the outcoupling of light from the film[50]. This effect can be clearly seen through a comparison of the steady-state emission to the long-lived component of the transient optical signal, which exhibit nearly identical lineshapes and relative intensities over a series of angles (Fig. S6). As discussed below, these species are also not observed in blends and as such are irrelevant to our discussion of CT dynamics.

Additional features corresponding to IOMs are observed in the momentum-resolved transient spectra and support our determination of the polariton lifetime. For example, under photoexcitation at 680 nm, we observe an additional dispersion feature near the IOM resonance at 525 nm in addition to the LP feature at 735 nm (Fig. 4c). The IOM feature is also short-lived (Fig. 4e) and exhibits decay dynamics that nearly identical to the values obtained at the LP probe wavelength (Fig. 4f). This response can be readily understood by inspection of the field profile for the IOM at 525 nm (Fig. 3c), which has significant spatial overlap with the organic layer. Transient photobleaching of the dye in the excited state modifies its effective refractive index, leading to small blue shifts in the dispersion of the IOM, consistent with previous findings[51]. As a result, the dynamics of the IOM-associated feature acts as a proxy for the excited state lifetime of the organic layer. As the IOM signal is free from artifacts stemming from optical Stark effects and background emission of weakly coupled species, it permits facile determination of the polariton lifetime.

IV. Tunable charge transfer from exciton-polaritons

We observe remarkably efficient CT from exciton-polaritons in the PM605-TCNQ/DBR configuration (Fig. 5b) using selective and direct LP excitation, significantly outperforming what is observed with either an uncoupled blend film or a PM605-TCNQ/Ag photonic structure. For example, there is no indication of the TCNQ⁻ signal in the transient optical data when selectively exciting the LP-WG mode at 640 nm in the PM605-TCNQ/Ag structure, consistent with its low quality factor and short lifetime that promotes ground state recombination over CT (Fig. 5a). In the kinetic trace extracted near the LP resonance (Fig. S9), we observe only a small peak with a width that is instrument response function limited, which we assign to the polariton. In contrast, under the same LP excitation conditions, the BSW hybrid mode on the DBR structure exhibits an additional long-lived feature with a lifetime corresponding to the measured decay of the TCNQ⁻ anion (Fig. S9). This effect persists even when the exciting momentum states have larger energetic separation from the reservoir states. Under PMCs at 705 nm, strong anion peaks at 750 nm and 850 nm can be seen in the

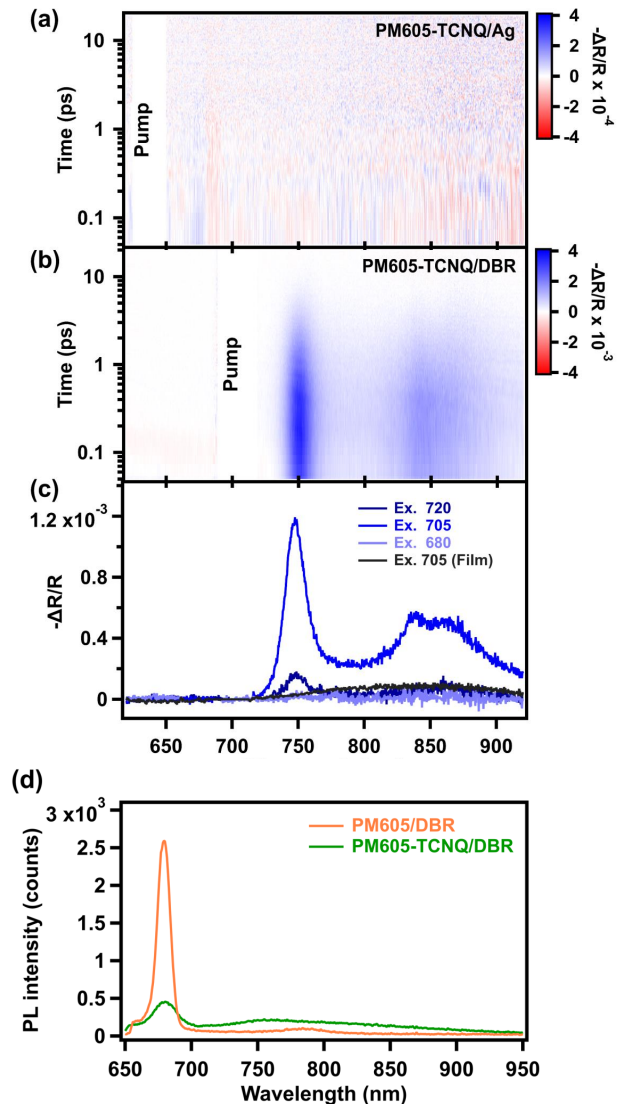


FIG. 5. Driving selective and efficient CT with long-lived BSW polaritons. (a) Transient reflection data of the strongly coupled PM605-TCNQ/Ag structure under selective LP excitation with suppressed CT. (b) Transient reflection data of PM605-TCNQ/DBR under direct LP excitation, achieving strong CT. (c) Comparative analysis of transient reflection data for PM605-TCNQ film and PM605-TCNQ/DBR under PMC (705 nm) and non-PMCs. (d) PL map showing LP emission quenching for the PM605-TCNQ/DBR structure compared to PM605/DBR under PMC at 633 nm.

transient optical data, which can be readily assigned to TCNQ⁻ states formed from photoexcited CT. We note that the spectral shape of the anion peaks is modified by the reflectivity spectrum of the DBR in the NIR, such that the strongest features are aligned with the modes of the photonic system.

Importantly, the intensity of the anion peaks is the highest when the pump matches the energy- and

momentum-resonance conditions of the LP. For pumping with constant momentum and a detuned energy from the polariton dispersion ((Fig. 5d), PMCs are not satisfied for LP excitation and the intensity of the TCNQ⁻ anion decreases significantly. We note that the response of the neat blend film, uncoupled to the cavity, is minimal at these pumping wavelengths indicating that hybrid mode plays a role in facilitating CT. Further evidence for the direct involvement of the hybrid mode in the CT process is obtained from photoluminescence measurements (Fig. 5d) in which a marked decrease of the LP emission is observed in the PM605-TCNQ/DBR structure compared to PM605/DBR under PMCs. This effect suggests quenching of the LP emission due to a competing CT channel. The magnitude of the PL quenching ($\sim 20\%$) permits a rough estimate of the CT time of ~ 85 fs using the lifetime of the LP in the neat PM605 film under identical pumping conditions (~ 350 fs). Consistent with this timescale, our data exhibit an instrument response limited (120 fs) rise in the anion feature. Similarly, it also suggests an explanation for the lack of an observed CT signal in the PM605-TCNQ/Ag photonic structure, for which the hybrid modes decay on time scales that are significantly faster than vibrationally mediated CT[52–55]. Finally, we confirm that the magnitude of the anion peak scales linearly with laser fluence, ruling out many-body or nonlinear effects(Fig. S10).

These results indicate that efficient charge transfer from an organic exciton-polariton can be achieved with a significantly reduced energetic driving force as compared to the bare exciton. Molecular charge transfer is driven by the energy difference between the lowest energy donor excited state (PM605 exciton or polariton state) and the LUMO level of the acceptor (TCNQ). Outside the cavity,

this value is fixed at 0.7 eV, a relatively large value compared to high performing optoelectronic systems[56, 57]. When strongly coupled to the photonic structure, efficient charge transfer is achieved for selective LP excitation with a driving force that is a function of the photon in-plane momentum. For example, charge transfer is greatly enhanced under PMC with 640 nm (Fig. S9) and 705 nm excitation (Fig. 5b), corresponding to an energetic driving force of 0.4 eV (0.3 eV lower than the exciton energy) and 0.2 eV (0.5 eV lower), respectively.

V. Conclusion

In conclusion, our work underscores the critical role of cavity configuration and excitation condition in optimizing the photochemical behavior of organic exciton-polaritons. Our work confirms that polariton-enhanced charge transfer reactions are indeed achievable, but basic, long-established frameworks governing molecular systems cannot be ignored. In most systems, the key parameters are selective excitation of polariton states via energy- and momentum-matching along with hybrid-state lifetimes that significantly exceed the timescales necessary for vibrationally-mediated incoherent charge transfer. As such, Bloch surface wave systems are promising platforms to explore polariton-driven photochemistry, though other promising systems such as lattice resonances may offer similar advantages. While polariton photochemistry is not the panacea that will enable systematic explorations of all relevant excited state processes, we verify that it is achievable under specific conditions.

-
- [1] C. Weisbuch, M. Nishioka, A. Ishikawa, and Y. Arakawa, Observation of the coupled exciton-photon mode splitting in a semiconductor quantum microcavity, *Physical review letters* **69**, 3314 (1992).
 - [2] J. Hopfield, Theory of the contribution of excitons to the complex dielectric constant of crystals, *Physical Review* **112**, 1555 (1958).
 - [3] S. Ghosh, R. Su, J. Zhao, A. Fieramosca, J. Wu, T. Li, Q. Zhang, F. Li, Z. Chen, T. Liew, *et al.*, Microcavity exciton polaritons at room temperature, *Photonics Insights* **1**, R04 (2022).
 - [4] J. Kasprzak, M. Richard, S. Kundermann, A. Baas, P. Jeambrun, J. M. J. Keeling, F. Marchetti, M. Szymańska, R. André, J. Staehli, *et al.*, Bose–einstein condensation of exciton polaritons, *Nature* **443**, 409 (2006).
 - [5] A. Amo, J. Lefrère, S. Pigeon, C. Adrados, C. Ciuti, I. Carusotto, R. Houdré, E. Giacobino, and A. Bramati, Superfluidity of polaritons in semiconductor microcavities, *Nature Physics* **5**, 805 (2009).
 - [6] K. G. Lagoudakis, M. Wouters, M. Richard, A. Baas, I. Carusotto, R. André, L. S. Dang, and B. Deveaud-Plédran, Quantized vortices in an exciton–polariton condensate, *Nature physics* **4**, 706 (2008).
 - [7] A. V. Zasedatelev, A. V. Baranikov, D. Urbonas, F. Scafrimuto, U. Scherf, T. Stöferle, R. F. Mahrt, and P. G. Lagoudakis, A room-temperature organic polariton transistor, *Nature Photonics* **13**, 378 (2019).
 - [8] J. A. Hutchison, A. Liscio, T. Schwartz, A. Canaguier-Durand, C. Genet, V. Palermo, P. Samorì, and T. W. Ebbesen, Tuning the work-function via strong coupling, *Advanced Materials* **25**, 2481 (2013).
 - [9] E. Orgiu, J. George, J. Hutchison, E. Devaux, J. Dayen, B. Doudin, F. Stellacci, C. Genet, J. Schachenmayer, C. Genes, *et al.*, Conductivity in organic semiconductors hybridized with the vacuum field, *Nature Materials* **14**, 1123 (2015).
 - [10] G. G. Rozenman, K. Akulov, A. Golombek, and T. Schwartz, Long-range transport of organic exciton-polaritons revealed by ultrafast microscopy, *ACS Photonics* **5**, 105 (2018).
 - [11] D. M. Coles, N. Somaschi, P. Michetti, C. Clark, P. G. Lagoudakis, P. G. Savvidis, and D. G. Lidzey, Polariton-mediated energy transfer between organic dyes in a

- strongly coupled optical microcavity, *Nature materials* **13**, 712 (2014).
- [12] M. Du, L. A. Martínez-Martínez, R. F. Ribeiro, Z. Hu, V. M. Menon, and J. Yuen-Zhou, Theory for polariton-assisted remote energy transfer, *Chemical science* **9**, 6659 (2018).
- [13] K. Georgiou, R. Jayaprakash, A. Othonos, and D. G. Lidzey, Ultralong-range polariton-assisted energy transfer in organic microcavities, *Angewandte Chemie* **133**, 16797 (2021).
- [14] B. Liu, X. Huang, S. Hou, D. Fan, and S. R. Forrest, Photocurrent generation following long-range propagation of organic exciton-polaritons, *Optica* **9**, 1029 (2022).
- [15] V. C. Nikolis, A. Mischok, B. Siegmund, J. Kublitski, X. Jia, J. Benduhn, U. Hörmann, D. Neher, M. C. Gather, D. Spoltore, *et al.*, Strong light-matter coupling for reduced photon energy losses in organic photovoltaics, *Nature communications* **10**, 3706 (2019).
- [16] R. Bhuyan, J. Mony, O. Kotov, G. W. Castellanos, J. Gomez Rivas, T. O. Shegai, and K. Börjesson, The rise and current status of polaritonic photochemistry and photophysics, *Chemical Reviews* **123**, 10877 (2023).
- [17] A. Mandal and P. Huo, Investigating new reactivities enabled by polariton photochemistry, *The journal of physical chemistry letters* **10**, 5519 (2019).
- [18] J. Yuen-Zhou and V. M. Menon, Polariton chemistry: Thinking inside the (photon) box, *Proceedings of the National Academy of Sciences* **116**, 5214 (2019).
- [19] J. A. Hutchison, T. Schwartz, C. Genet, E. Devaux, and T. W. Ebbesen, Modifying chemical landscapes by coupling to vacuum fields, *Angewandte Chemie International Edition* **51**, 1592 (2012).
- [20] B. Munkhbat, M. Wersäll, D. G. Baranov, T. J. Antosiewicz, and T. Shegai, Suppression of photo-oxidation of organic chromophores by strong coupling to plasmonic nanoantennas, *Science advances* **4**, eaas9552 (2018).
- [21] A. J. Ward, A. Ruseckas, M. M. Kareem, B. Ebenhoch, L. A. Serrano, M. Al-Eid, B. Fitzpatrick, V. M. Rotello, G. Cooke, and I. D. Samuel, The impact of driving force on electron transfer rates in photovoltaic donor-acceptor blends, *Advanced Materials* **27**, 2496 (2015).
- [22] T. Unger, S. Wedler, F.-J. Kahle, U. Scherf, H. Bässler, and A. Köhler, The impact of driving force and temperature on the electron transfer in donor-acceptor blend systems, *The Journal of Physical Chemistry C* **121**, 22739 (2017).
- [23] B. K. Paul, A. Samanta, S. Kar, and N. Guchhait, Evidence for excited state intramolecular charge transfer reaction in donor-acceptor molecule 5-(4-dimethylamino-phenyl)-penta-2, 4-dienoic acid methyl ester: Experimental and quantum chemical approach, *Journal of luminescence* **130**, 1258 (2010).
- [24] C. Delesma, C. Amador-Bedolla, M. Robles, and J. Muñoz, Photoisomerization and its effect in the optoelectronic properties of organic photovoltaic materials: A quantum chemistry study, *Journal of Photochemistry and Photobiology A: Chemistry* **409**, 113155 (2021).
- [25] C. Schäfer, M. Ruggenthaler, H. Appel, and A. Rubio, Modification of excitation and charge transfer in cavity quantum-electrodynamical chemistry, *Proceedings of the National Academy of Sciences* **116**, 4883 (2019).
- [26] H. S. Kim, S. H. Lee, S. Yoo, and C. Adachi, Understanding of complex spin up-conversion processes in charge-transfer-type organic molecules, *Nature communications* **15**, 2267 (2024).
- [27] C. Deibel, T. Strobel, and V. Dyakonov, Role of the charge transfer state in organic donor-acceptor solar cells, *Advanced materials* **22**, 4097 (2010).
- [28] R. A. Marcus, On the theory of oxidation-reduction reactions involving electron transfer. i, *The Journal of chemical physics* **24**, 966 (1956).
- [29] H. Sumi, Adiabatic versus non-adiabatic electron transfer, in *Electron Transfer in Chemistry* (John Wiley & Sons, Ltd) Chap. 2, pp. 64–108.
- [30] B. Hou, M. Thoss, U. Banin, and E. Rabani, Incoherent nonadiabatic to coherent adiabatic transition of electron transfer in colloidal quantum dot molecules, *Nature Communications* **14**, 3073 (2023).
- [31] D. G. Baranov, M. Wersall, J. Cuadra, T. J. Antosiewicz, and T. Shegai, Novel nanostructures and materials for strong light-matter interactions, *Acs Photonics* **5**, 24 (2018).
- [32] E. Michail, K. Rashidi, B. Liu, G. He, V. M. Menon, and M. Y. Sfeir, Addressing the dark state problem in strongly coupled organic exciton-polariton systems, *Nano Letters* **24**, 557 (2024).
- [33] C. Climent, D. Casanova, J. Feist, and F. J. Garcia-Vidal, Not dark yet for strong light-matter coupling to accelerate singlet fission dynamics, *Cell Reports Physical Science* **3** (2022).
- [34] A. B. Grafton, A. D. Dunkelberger, B. S. Simpkins, J. F. Triana, F. J. Hernández, F. Herrera, and J. C. Owrutsky, Excited-state vibration-polariton transitions and dynamics in nitroprusside, *Nature Communications* **12**, 214 (2021).
- [35] T. Khazanov, S. Gunasekaran, A. George, R. Lomlu, S. Mukherjee, and A. J. Musser, Embrace the darkness: An experimental perspective on organic exciton-polaritons, *Chemical Physics Reviews* **4** (2023).
- [36] A. Dutta, V. Tiainen, I. Sokolovskii, L. Duarte, N. Markešević, D. Morozov, H. A. Qureshi, S. Pikker, G. Groenhof, and J. J. Toppari, Thermal disorder prevents the suppression of ultra-fast photochemistry in the strong light-matter coupling regime, *Nature Communications* **15**, 6600 (2024).
- [37] B. Liu, V. M. Menon, and M. Y. Sfeir, Ultrafast thermal modification of strong coupling in an organic microcavity, *APL Photonics* **6** (2021).
- [38] M. Litinskaya, P. Reineker, and V. M. Agranovich, Fast polariton relaxation in strongly coupled organic microcavities, *Journal of luminescence* **110**, 364 (2004).
- [39] T. Schwartz, J. A. Hutchison, J. Léonard, C. Genet, S. Haacke, and T. W. Ebbesen, Polariton dynamics under strong light-molecule coupling, *ChemPhysChem* **14**, 125 (2013).
- [40] G. H. Lodden and R. J. Holmes, Electrical excitation of microcavity polaritons by radiative pumping from a weakly coupled organic semiconductor, *Physical Review B—Condensed Matter and Materials Physics* **82**, 125317 (2010).
- [41] M. Liscidini, D. Gerace, D. Sanvitto, and D. Bajoni, Guided bloch surface wave polaritons, *Applied Physics Letters* **98** (2011).
- [42] S. Pirotta, M. Patrini, M. Liscidini, M. Galli, G. Dacarro, G. Canazza, G. Guizzetti, D. Comoretto, and D. Bajoni, Strong coupling between excitons in organic semiconductors and bloch surface waves, *Applied Physics Letters* **104** (2014).

- [43] F. Barachati, A. Fieramosca, S. Hafezian, J. Gu, B. Chakraborty, D. Ballarini, L. Martinu, V. Menon, D. Sanvitto, and S. Kéna-Cohen, Interacting polariton fluids in a monolayer of tungsten disulfide, *Nature nanotechnology* **13**, 906 (2018).
- [44] S. Bhaskar, P. Das, V. Srinivasan, S. Bhaktha BN, and S. S. Ramamurthy, Bloch surface waves and internal optical modes-driven photonic crystal-coupled emission platform for femtomolar detection of aluminum ions, *The Journal of Physical Chemistry C* **124**, 7341 (2020).
- [45] S. M. G. Mousavi-Kiasari, K. Rashidi, D. Fathi, H. Taleb, S. M. Mirjalili, and V. Faramarzi, Computational design of highly-sensitive graphene-based multilayer spr biosensor, in *Photonics*, Vol. 9 (MDPI, 2022) p. 688.
- [46] G. Lerario, D. Ballarini, A. Fieramosca, A. Cannavale, A. Genco, F. Mangione, S. Gambino, L. Dominici, M. De Giorgi, G. Gigli, *et al.*, High-speed flow of interacting organic polaritons, *Light: Science & Applications* **6**, e16212 (2017).
- [47] S. J. Hall, P. J. Budden, A. Zats, and M. Y. Sfeir, Optimizing the sensitivity of high repetition rate broadband transient optical spectroscopy with modified shot-to-shot detection, *Review of Scientific Instruments* **94** (2023).
- [48] A. Hayat, C. Lange, L. A. Rozema, A. Darabi, H. M. Van Driel, A. M. Steinberg, B. Nelsen, D. W. Snoke, L. N. Pfeiffer, and K. W. West, Dynamic stark effect in strongly coupled microcavity exciton polaritons, *Physical Review Letters* **109**, 033605 (2012).
- [49] T. LaMountain, J. Nelson, E. J. Lenferink, S. H. Amsterdam, A. A. Murthy, H. Zeng, T. J. Marks, V. P. Dravid, M. C. Hersam, and N. P. Stern, Valley-selective optical stark effect of exciton-polaritons in a monolayer semiconductor, *Nature communications* **12**, 4530 (2021).
- [50] B. S. Simpkins, Z. Yang, A. D. Dunkelberger, I. Vurgaftman, J. C. Owrutsky, and W. Xiong, Comment on “isolating polaritonic 2d-ir transmission spectra”, *The Journal of Physical Chemistry Letters* **14**, 983 (2023).
- [51] S. Renken, R. Pandya, K. Georgiou, R. Jayaprakash, L. Gai, Z. Shen, D. G. Lidzey, A. Rao, and A. J. Musser, Untargeted effects in organic exciton-polariton transient spectroscopy: A cautionary tale, *The Journal of Chemical Physics* **155** (2021).
- [52] M. Wang, M. Hertzog, and K. Börjesson, Polariton-assisted excitation energy channeling in organic heterojunctions, *Nature communications* **12**, 1874 (2021).
- [53] C. A. DelPo, S.-U.-Z. Khan, K. H. Park, B. Kudisch, B. P. Rand, and G. D. Scholes, Polariton decay in donor-acceptor cavity systems, *The Journal of Physical Chemistry Letters* **12**, 9774 (2021).
- [54] X. Hong, J. Kim, S.-F. Shi, Y. Zhang, C. Jin, Y. Sun, S. Tongay, J. Wu, Y. Zhang, and F. Wang, Ultrafast charge transfer in atomically thin mos₂/ws₂ heterostructures, *Nature nanotechnology* **9**, 682 (2014).
- [55] X. Chen, X. Zhang, X. Xiao, Z. Wang, and J. Zhao, Recent developments on understanding charge transfer in molecular electron donor-acceptor systems, *Angewandte Chemie International Edition* **62**, e202216010 (2023).
- [56] D. B. Rodovsky, J. Peet, N. Shao, J. D. Azoulay, G. C. Bazan, N. Drolet, Q. Wu, and M. Y. Sfeir, Quantifying the relationship between the maximum achievable voltage and current levels in low-bandgap polymer photovoltaics, *The Journal of Physical Chemistry C* **117**, 25955 (2013).
- [57] D. Qian, Z. Zheng, H. Yao, W. Tress, T. R. Hopper, S. Chen, S. Li, J. Liu, S. Chen, J. Zhang, X.-K. Liu, B. Gao, L. Ouyang, Y. Jin, G. Pozina, I. A. Buyanova, W. M. Chen, O. Inganäs, V. Coropceanu, J.-L. Bredas, H. Yan, J. Hou, F. Zhang, A. A. Bakulin, and F. Gao, Design rules for minimizing voltage losses in high-efficiency organic solar cells, *Nature Materials* **17**, 703 (2018).

VI. Materials and methods

A. Sample preparation

The two distributed Bragg reflectors (DBRs), composed of 6 pairs of Si₃N₄(110, nm)/SiO₂(146, nm), were prepared on a 0.15 mm thick BK7 substrate using plasma-enhanced chemical vapor deposition (PECVD), resulting in a stop-band centered at 860 nm. Subsequently, an 80 nm-thick film of PM605 on the first one and PM605-TCNQ 1:1 on the second one embedded both in Polymethyl Methacrylate (PMMA) polymer matrix were spin-coated onto the DBRs.

The metal cavities were prepared by depositing a 2 nm Germanium layer and a 30 nm silver layer using an e-beam evaporator on a 0.15 mm thick BK7 substrate, followed by spin-coating a PM605-TCNQ blend embedded in a PMMA polymer matrix, resulting in a thickness of 150 nm.

B. Time-resolved reflection spectroscopy

A pump-probe reflection geometry was employed using the Kretschmann–Raether attenuated total reflection method. A Yb:KGW amplified laser system (Light Conversion, Carbide CB3) operating at a center wavelength of 1030 nm delivered pulses at a repetition rate of 90 kHz. An optical parametric amplifier (OPA) (Light Conversion, Orpheus-F) generated the pump pulse, spanning from UV to NIR. A yttrium aluminum garnet (YAG) crystal produced the probe light with a supercontinuum spectrum covering the visible (VIS) and near-infrared (NIR) ranges. In the Kretschmann-Raether configuration, both pump and probe pulses propagated through a glass prism. The pump-probe delay was mechanically controlled using a delay stage and retroreflector before generating white light. Broadband quarter-waveplates and polarizers were employed to regulate the intensity and polarization direction of both the pump and probe beams. A fast line-scan camera (Teledyne, e2V Octoplus USB) with a burst modulation scheme facilitated multi-channel shot-to-shot detection.

C. Angle-resolved reflection spectroscopy

The angle-resolved reflectivity was measured using a home-build Fourier space imaging setup consisting of a tungsten halogen lamp. White light from the lamp was

focused onto the sample using an oil immersion objective lens (100x, 1.4 NA, Olympus). Immersion oil facilitated the attachment of the glass substrate to the objective lens. Reflected light was collected through the same microscope objective and directed to the back focal plane of the imaging objective. The light at the back focal plane was then directed through a monochromator (Acton SpectraPro SP-2500, Princeton Instruments) and detected by an electron-multiplying charge-coupled device (EMCCD) camera (PIXIS: 256, Princeton Instruments).

D. Electrochemistry methods

Spectroelectrochemistry measurements were conducted using a home-built setup. The sample was irradi-

ated with collimated white light (200 nm - 2.5 μm) and the emitted light was collected with a CCD spectrometer. The sample was placed in a 2 mm electrochemistry cell equipped with a pre-assembled mesh working electrode, a Pt counter electrode, and an Ag/Ag⁺ pseudo reference electrode. Cyclic voltammetry measurements were performed in a three-electrode configuration cell. The setup included an Ag/Ag⁺ pseudo reference electrode (referenced to the Fc/Fc⁺ couple), a glassy carbon working electrode, and a platinum counter electrode. Cyclic voltammetry and spectroelectrochemistry measurements were carried out in 1 mM and 0.1 mM analyte solutions, respectively, under an inert atmosphere maintained by a constant argon flux. Acetonitrile (anhydrous, 99.8%) was used as the solvent, with [nBu₄N]PF₆ serving as the supporting electrolyte.